

# **SANDIA REPORT**

SAND2008-5185  
Unlimited Release  
Printed August 2008

## **The Sandia MEMS Passive Shock Sensor: FY08 Failure Analysis Activities**

Jeremy A. Walraven, Michael S. Baker, Jonathan W. Wittwer, David S. Epp, Matthew R. Brake, Rebecca C. Clemens, John A. Mitchell.

Prepared by  
Sandia National Laboratories  
Albuquerque, New Mexico 87185 and Livermore, California 94550

Sandia is a multiprogram laboratory operated by Sandia Corporation,  
a Lockheed Martin Company, for the United States Department of Energy's  
National Nuclear Security Administration under Contract DE-AC04-94AL85000.

Approved for public release; further dissemination unlimited.



Issued by Sandia National Laboratories, operated for the United States Department of Energy by Sandia Corporation.

**NOTICE:** This report was prepared as an account of work sponsored by an agency of the United States Government. Neither the United States Government, nor any agency thereof, nor any of their employees, nor any of their contractors, subcontractors, or their employees, make any warranty, express or implied, or assume any legal liability or responsibility for the accuracy, completeness, or usefulness of any information, apparatus, product, or process disclosed, or represent that its use would not infringe privately owned rights. Reference herein to any specific commercial product, process, or service by trade name, trademark, manufacturer, or otherwise, does not necessarily constitute or imply its endorsement, recommendation, or favoring by the United States Government, any agency thereof, or any of their contractors or subcontractors. The views and opinions expressed herein do not necessarily state or reflect those of the United States Government, any agency thereof, or any of their contractors.

Printed in the United States of America. This report has been reproduced directly from the best available copy.

Available to DOE and DOE contractors from

U.S. Department of Energy  
Office of Scientific and Technical Information  
P.O. Box 62  
Oak Ridge, TN 37831

Telephone: (865)576-8401  
Facsimile: (865)576-5728  
E-Mail: [reports@adonis.osti.gov](mailto:reports@adonis.osti.gov)  
Online ordering: <http://www.osti.gov/bridge>

Available to the public from

U.S. Department of Commerce  
National Technical Information Service  
5285 Port Royal Rd  
Springfield, VA 22161

Telephone: (800)553-6847  
Facsimile: (703)605-6900  
E-Mail: [orders@ntis.fedworld.gov](mailto:orders@ntis.fedworld.gov)  
Online order: <http://www.ntis.gov/help/ordermethods.asp?loc=7-4-0#online>



SAND2008-5185  
Unlimited Release  
Printed August 2008

# The Sandia MEMS Passive Shock Sensor: FY08 Failure Analysis Activities

Jeremy A. Walraven  
Microsystems Failure Analysis

Michael S. Baker, Jonathan W. Wittwer  
MEMS Technologies

David S. Epp, Matthew R. Brake  
Applied Mechanics

Rebecca C. Clemens, John A. Mitchell  
Electromechanical Engineering

Sandia National Laboratories  
P.O. Box 5800  
Albuquerque, NM 87185-MS1081

## **Abstract**

This report summarizes failure analysis activities performed on various designs of the MEMS based Passive Shock Sensor (PSS). The failure analysis activities in this report focus on identifying root cause of failures observed at both die and package levels. The findings from these failure analyses have and will lead to implementation of corrective actions focusing on maturing the MEMS-based PSS and meeting product deliverables and milestones.

## **Acknowledgments**

The authors gratefully acknowledge funding and support from the Embedded Evaluation program run by Bob Paulsen and Paul Yoon, the Campaign 6 program run by T.Y. Chu, the Campaign 5 program run by Davina Kwon, the DSW Campaign run by Mike Sjulín and Russ Miller, and the overall support and guidance of Mary Gonzales. Without this support the accomplishments documented here would have not been possible. Finally, special thanks go to Patricia Oliver for helping to create the form and legibility of the report.

# Contents

<b>1. INTRODUCTION.....</b>	<b>9</b>
1.1 Motivation and Background .....	9
1.2 Objectives .....	9
<b>2. APPROACH.....</b>	<b>11</b>
2.1 Failure Analysis: Passive Shock Sensor Dice.....	11
2.2 Failure Analysis: Passive Shock Sensor Packaged Components.....	13
<b>3. FAILURE ANALYSIS RESULTS .....</b>	<b>15</b>
3.1 Passive Shock Switch Failure Analysis: Die Level.....	15
3.1.1 Dimple Gap Analysis.....	15
3.1.2 Metallization Shorting via Sputter Deposition .....	16
3.1.3 Thick Polysilicon Process Development .....	19
3.1.4 Silicon Nitride Isolation Process Development .....	21
3.2 Passive Shock Switch Failure Analysis: Package Level .....	25
3.2.1 Self-Test and Shock Test .....	26
3.2.2 Thermal Testing .....	32
<b>4. CONCLUSIONS .....</b>	<b>35</b>
<b>5. REFERENCES.....</b>	<b>37</b>

## Figures

Figure 2-1. Schematic representation of a TIVA system using a scanning optical microscope (SOM). .....	12
Figure 2-2. Schematic of the TIVA technique employed across two conductive lines. Note the lack of TIVA when the laser is scanned over power lines in the region outside of the particle versus the response of the laser scanned over the particle causing a short.....	13
Figure 3-1. Dimple contact with the moveable mass.....	15

Figure 3-2. a) Optical image of a mechanically cross-sectioned as-fabricated PSS device showing the dimple in very close proximity to the moveable mass, b) FIB analysis showing an as-fabricated gap spacing of $\sim 0.24 \mu\text{m}$ , smaller than the $0.40 \mu\text{m}$ design.....	16
Figure 3-3. a) Reflected light image of a PSS device post metal deposition, b) TIVA image using a 1064 nm laser with 1 $\mu\text{A}$ applied bias. Note the arrows identify sites of interest where an electrical short exists. ....	17
Figure 3-4. a) SEM analysis of a thermal actuator edge does not shadow the underlying poly 0 structure indicating metal is contacting poly 0, b) metal contact confirmed on the right portion of the image. Note the dark contrast on the bottom of the left side (absence of metal) and the bright contrast on the right side (presence of metal). ....	18
Figure 3-5. a) SEM image of a poly 4 cover removed exposing a moveable shuttle, b) SEM image measuring 17 $\mu\text{m}$ of metal penetration underneath the poly 4 cover. ....	18
Figure 3-6. a) SEM image showing Ti and Pt metal thickness on the top and side of a bond pad. Sidewall thickness measurement was taken at the bottom. b) SEM image with same thickness measurements but at a different location on the sidewall.....	19
Figure 3-7. a) Optical image of a released thick poly test structure, b) IR image of a released moveable shuttle, c) small dark spots are observed inside the etch release holes of the moveable shuttle (arrows).....	19
Figure 3-8. a) Optical image of a moveable shuttle with the poly 4 cover removed (note the small particles in proximity to the etch release holes), b) SEM of the same area showing the structures in better detail (circle denotes EDS sample area). ....	20
Figure 3-9. a) SEM image of the material found in an etch release hole, b) its corresponding EDS spectra indicating the particle is silicon. ....	20
Figure 3-10. a) Schematic cross-section illustrating key-hole defect, b) cross-section partially through the etch release hole (note the presence of the structure), and c) a cross-section $\sim 3/4$ through an etch release hole in the moveable shuttle showing the formation of the silicon “stalactite”. ....	21
Figure 3-11. a) Nitride isolation dimple cuts on tensile test structures. Arrows indicate the nitride dimple cut and backfill; b) Schematic of nitride isolation anchors which mechanical tie Poly 1 & 2 to Poly 3 (red line indicates electrical path isolation of left Poly 1 & 2 from Poly 3) .....	22
Figure 3-12. a & b), Optical images showing the results of a pull test on the nitride isolation structures. Note only one sample failed at the polysilicon whereas the rest failed along the silicon nitride/polysilicon interface.....	23
Figure 3-13. Fracture surfaces of test structures with silicon nitride isolation a) failure at the silicon nitride/poly interface, streaking b) fracture on the polysilicon layer, c & d) failure at the silicon nitride/poly interface.....	24
Figure 3-14. a) Short nitride isolation cut interface with a small polysilicon grain missing indicating polysilicon delamination, b) fracture of the polysilicon with the nitride still adhered to the poly, streaking; c) nitride delamination on a 15 $\mu\text{m}$ long isolation cut (note the extruded grains), and d), nitride delamination. ....	25

Figure 3-15. Delidding procedure demonstrated on a) PSS mounted on a board, b) razor blade perforating the seal along the lid/solder ring, and c) lid removed exposing the die.....	27
Figure 3-16. a) Delidded and exposed die from self-test, b) close-up of device D. ....	28
Figure 3-17. Poly 4 cover plate removal process by a) strategic FIB cut layout, b) Pt GIS insertion, c) Pt deposition, and d) lid removal. Lid removed on part X1043. ....	30
Figure 3-18. a) Poly 4 cover removed exposing the underlying proof mass, b) closer examination of the thermal actuator/proof mass contact. ....	31
Figure 3-19. a) Bi-stable mass removed, exposing the underlying the substrate and anchors (arrows), b) SEM analysis of the portion of the polysilicon bi-stable mass underneath the anchors (arrow), no sign of damage, rubbing, or gouging was observed. ....	31
Figure 3-20. a) Possible contamination spot on the substrate coincident with the poly 1 dimple shown in b).....	31
Figure 3-21. a) Self-test sample X1031 with the poly 4 cover removed, and b) close-up view of the bi-stable mechanism. ....	32
Figure 3-22: a) Bi-stable mass removed exposing the substrate, and b) analysis near an anchor did not reveal any dark spots.....	32
Figure 3-23. a & b) Dark Field optical microscopy exposing contamination on the substrate of a thermally tested PSS component. ....	33
Figure 3-24. a & b) SEM analysis of contacts did not reveal any welding or other defects. ....	33
Figure 3-25. a) SEM image of the poly 0 substrate underneath the bi-stable mass showing a small dark spot coincident with the poly 1 dimple location, b) poly 1 dimple on the bottom of the bi-stable mass. ....	34

# Acronyms

CIVA	Charge-induced voltage alteration
DUT	Device under test
EDS	Energy dispersive x-ray analysis
FA	Failure analysis
FIB	Focused ion beam
GIS	Gas insertion system
IC	Integrated circuit
IR	Infrared
LIVA	Light-induced voltage alteration
MEMS	Micro electromechanical system
OM	Optical microscopy
PSS	Passive shock sensor
SEM	Scanning electron microscopy (or microscope)
SOM	Scanning optical microscope
SUMMiT	Sandia ultra-planar MEMS technology
TIVA	Thermally induced voltage alteration
TRL	Technology readiness level

# 1. Introduction

## 1.1 Motivation and Background

Failure analysis (FA) activities on the passive shock sensor (PSS) device were initiated in FY07 and continued into FY08. The motivation behind performing failure analysis was to identify and determine the root cause of failure on the PSS components at the die and packaged states. By identifying the root cause of failure, corrective actions improving device performance and reliability could be made in a timely manner. Through these FA activities and improvements, PSS components can make their product deliverables and project milestones.

## 1.2 Objectives

After demonstrating “proof of concept” in FY06 (see [1]), achieving technology readiness level (TRL) 4, and identifying packaging concepts, the goal for the PSS component was to mature the micro electromechanical systems (MEMS)-based shock sensor to TRL 6. To advance to this level of technology readiness, failure modes at the fabrication level (die) as well as the packaging level had to be identified and corrective actions implemented. The objective of performing failure analysis on these PSS components was to identify the root cause of failure and implement a means of corrective action. The objectives sought during the failure analysis activities were:

1. Identify the location of the failure,
2. Identify the root cause of failure, and
3. Provide feedback aimed at improving device performance.

Through failure analysis, a better understanding of the shock sensor’s capabilities and limitations can be made, and efforts to improve upon those limitations can be addressed. It is through these analyses and improvements that a more robust and better functional PSS component can be fabricated, assembled, and delivered.



## 2. Approach

Failure analysis was performed on PSS devices from fabrication and testing, board level testing, and packaged/assembled modules. This section briefly describes the failure analysis approaches, tools, and techniques used to examine failed PSS components. The same toolsets used to analyze PSS devices at the die level are used to analyze them at the board level or packaged level as well. The main differences focus on providing electrical stimulus. At the die level, the electrical stimulus is provided by probes, and at the package level, it is provided through the packaging interconnects and bond wires. [2]

### 2.1 Failure Analysis: Passive Shock Sensor Dice

Die level failure analysis was performed on various versions of the PSS component including revisions 2, 3, 4, 5, and 6. At the time of this writing, only revisions 2, 3, and 4 have been documented in publications (see [1], [3], and [4]). Many of these activities involve issues with device fabrication. Such die level analyses included PSS dimple gaps, dimple contact/friction, metal deposition shorting via sputter deposition, structural analysis of thick poly, and nitride isolation (electrical and mechanical). Many of the failed devices listed above were compared to functional control devices (for functional assessment) and/or to designed fabrication protocols (for design and film thickness assessment).

Conventional failure analysis techniques such as bright field optical microscopy (OM), scanning electron microscopy (SEM), electrical stimulus (I-V characterization), and focused ion beam (FIB) cross-sectioning were used. These techniques were employed to measure film thicknesses, perform structural analyses, and electrically stimulate the part. Other techniques such as Thermally Induced Voltage Alteration (TIVA) were used to identify electrical shorts. The physics of TIVA [5] for integrated circuit (IC) examination employs the constant-current biasing method used in Charge-Induced Voltage Alteration (CIVA) [6] and Light-Induced Voltage Alteration (LIVA) [7]. The constant-current biasing approach provides an extremely sensitive method for detection of subtle changes in the IC or MEMS power demand. In TIVA, localized heating changes the resistance of a short and the effects of this resistance change on the power demands of the entire IC are used to produce an image. Power consumption of a short depends upon the resistance of the short and its location in the IC. For example, a  $V_{DD}$  (power) to  $V_{SS}$  (ground) short may dissipate more power than a short between two signal lines. If the short is of a metallic nature, the increase in temperature increases the resistance of the short, thereby reducing the power demands of the IC. The change in resistance of a short with heating from the scanned laser can be expressed by [8]:

$$\rho = \rho_0 (1 + \alpha(T-T_0))$$

where  $\rho$  is the resistivity of the short,  $\rho_0$  is the resistivity of the short at  $T_0$ ,  $\alpha$  is the temperature coefficient of resistivity,  $T$  is the temperature, and  $T_0$  is the steady-state or reference temperature. When the region of interest is “heated,” localized temperature variations of 5 – 50°C are realized. MEMS components often get hotter than their IC counterparts (using the same laser power) due

to their thermally isolated nature. MEMS structures are typically surrounded by silicon nitride, silicon oxide, or air. Therefore less laser power can be used when performing TIVA analysis on a MEMS component. For the PSS device, the metalized contacts and are surrounded by the packaging environment when in the open position, and are touching a contact bar when in the closed position. Other structures, such as the power lines and thermal actuators, are fabricated underneath a poly 4 cover plate and should be electrically isolated.

A schematic of a TIVA setup is shown in Figure 2-1 where the DUT (or device under test) is the MEMS component. For simple powering procedures, the switch matrix can be replaced with either probes or a switch box.

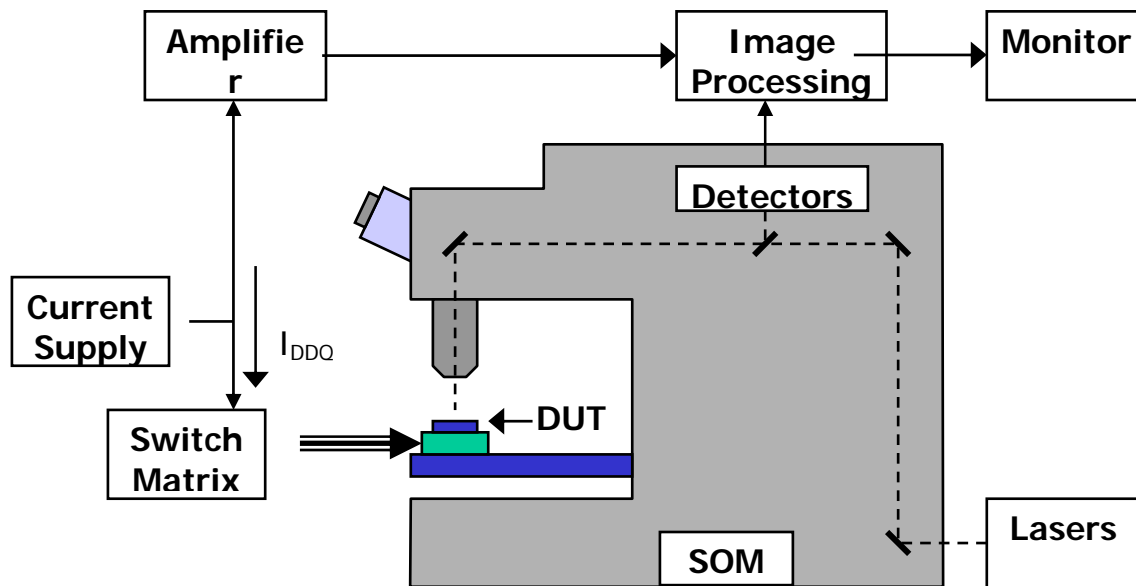


**Figure 2-1. Schematic representation of a TIVA system using a scanning optical microscope (SOM).**

When localizing shorts in signal lines the MEMS device must be biased (statically) with sufficient potential to “activate” the short. In MEMS structures, if particles or other materials are causing a short between active power lines, the change in resistance of the short when exposed to the laser can be readily observed. A schematic illustrating the TIVA technique (using a 1064 nm laser) employed on a particle-induced short between two conductive lines is shown in Figure 2-2.

Application of TIVA to MEMS presents some special opportunities. Because some MEMS structures are thermally isolated from the substrate of the MEMS device, the structures can be easily heated with much lower power than when TIVA is applied to ICs [9]. In fact, some devices require care to avoid overheating and possible damage to the MEMS structure by high temperature alteration of the thermally isolated components. Additionally, a number of MEMS devices do not have active IC structures, i.e., Si diffusions. With these structures there is no

concern of photocurrent effects swamping out the TIVA signals. Therefore, shorter-wavelength lasers with better spatial resolution can be used for TIVA images. The improved spatial resolution can also be seen in the reflected light images used for registration. The results of these analyses are discussed in Section 3.

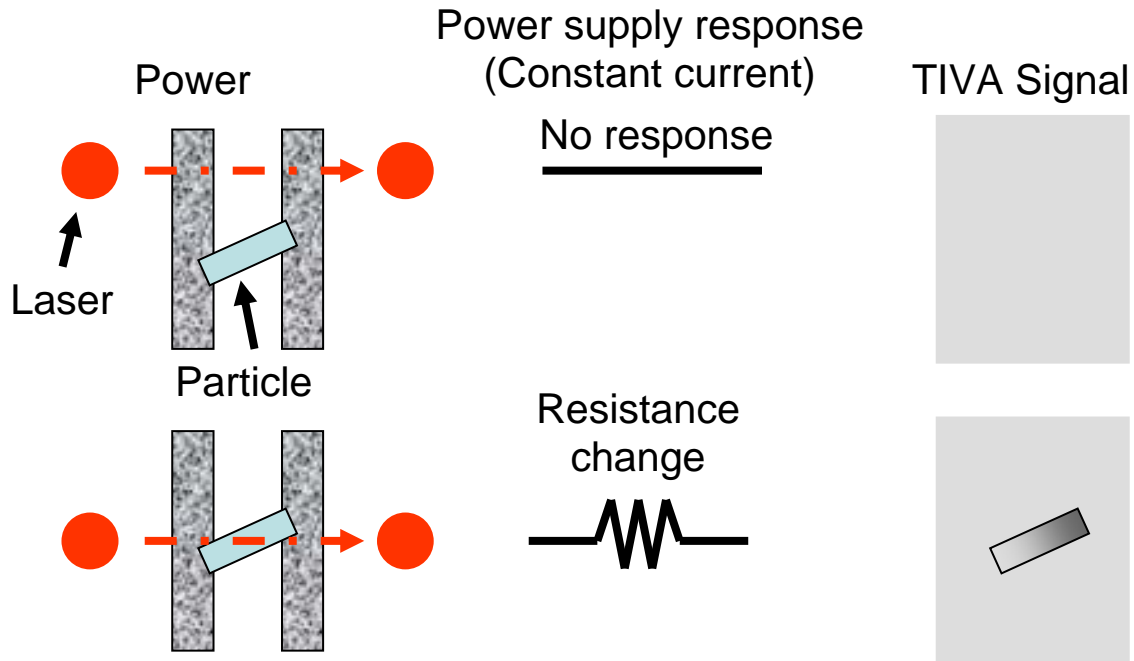


**Figure 2-2. Schematic of the TIVA technique employed across two conductive lines. Note the lack of TIVA when the laser is scanned over power lines in the region outside of the particle versus the response of the laser scanned over the particle causing a short.**

## 2.2 Failure Analysis: Passive Shock Sensor Packaged Components

Package level failure analyses were performed on devices tested under shock, vibration, and self-test conditions. These tests are discussed in detail in [4][10]. Examinations of the failed devices were compared to a control or functional PSS component of the same type. Such failures include electrical shorting introduced via packaging, and failures from shock, vibration, and self-test. These failures are typically identified as stuck-open or stuck-closed where the moveable shuttle is either in a fixed closed position (electrical contact is continuously made) or fixed open position (where the moveable shuttle cannot make electrical contact). On board-level and packaged-level components, the devices were electrically stimulated using the appropriate test connector and a laptop computer.



### 3. Failure Analysis Results

In this section we summarize findings from failure analysis activities performed on both die- and package-level PSS components. As this document pertains solely to the failure analysis activities, see more detailed discussions accounting for packaging, design in references [4] and [10].

#### 3.1 Passive Shock Switch Failure Analysis: Die Level

Failure analysis activities for PSS components include dimple gap analysis, dimple contact and/or friction, sputter metal deposition shorting, structural analysis of thick poly, and nitride isolation (electrical and mechanical). Many of the failed devices listed above were compared to functional control devices (for accurate functional assessment) or compared to designed fabrication protocols (for design and fabrication materials protocols). The PSS device consists of two moving thermal actuators, a latching mechanism to keep the contact bar in place, and a moveable proof mass. Images of the structure are shown later in the report.

##### 3.1.1 Dimple Gap Analysis

Failure analysis and design assessment of Rev 3 PSS components was performed to understand the cause of shuttle sticking. As discussed in a previous PSS report [3], the dimple 3 structure was identified as rubbing against the top portion of the moveable mass as shown in Figure 3-1. This rubbing introduced friction into the device causing the device to have altered open and closure characteristics.

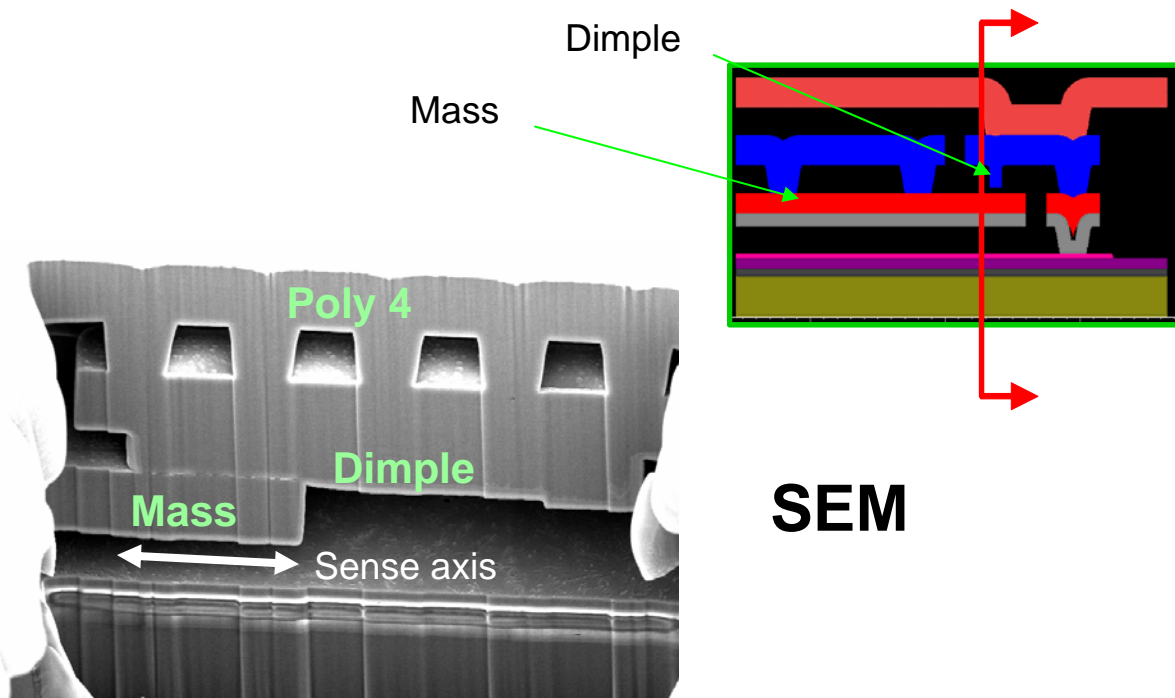
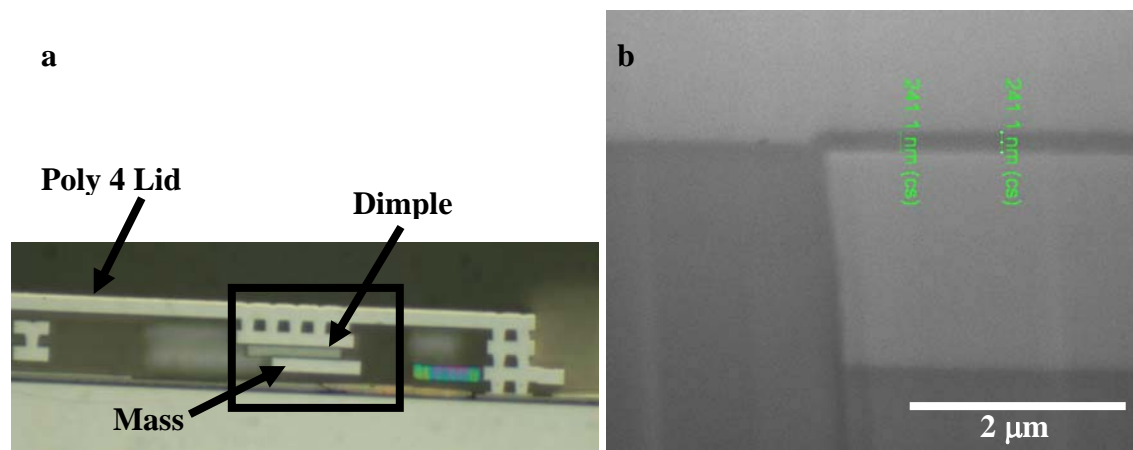


Figure 3-1. Dimple contact with the moveable mass.

Further analysis of the same mass and dimple via FIB cross-section and mechanical cross-section showed a gap spacing of  $\sim 0.24 \mu\text{m}$  instead of the designed specification of  $0.40 \mu\text{m}$ . This reduction in gap spacing along with other potential factors such as residual stress in the surrounding polysilicon structures and z-axis deflection lead to dimple contact and rubbing.

As shown in the FIB cross-section and mechanically polished optical image in Figure 3-2, the gap spacing of  $0.24 \mu\text{m}$  is caused by insufficient backfill from the sacrificial oxide deposition process. Analysis of blank wafers subjected to the same thin-film processing showed an oxide thickness of  $0.40 \mu\text{m}$ . This result confirms the change in surface topography introduces thinning of the sacrificial oxide in the dimple region creating the smaller gap spacing. The reduced gap spacing clearly makes the PSS component more susceptible to rubbing and sticking failures and/or significantly alters the PSS sensing capabilities. These failure analysis efforts led to revised designs with no dimples, effectively increasing the gap spacing between the oxide cut and the proof mass.



**Figure 3-2. a) Optical image of a mechanically cross-sectioned as-fabricated PSS device showing the dimple in very close proximity to the moveable mass, b) FIB analysis showing an as-fabricated gap spacing of  $\sim 0.24 \mu\text{m}$ , smaller than the  $0.40 \mu\text{m}$  design.**

### 3.1.2 Metallization Shorting via Sputter Deposition

Top-down sputter deposition processes were investigated on Revision 4 dice as a means to improve sidewall metal coverage on the PSS devices. This top-down process also simplified a previous metallization process (evaporation) that required die fixtures. The fixtures created a large number of particles which subsequently led to device failures. This new metallization process and failure analysis was also implemented on Revision 4 dice in order to verify and study poly 4 shadow masks in proximity to bond pads, traces, and other structure elements at risk of shorting. The metallization process consists depositing  $50 \text{ nm}$  of Titanium (Ti) and  $400 \text{ nm}$  of Platinum (Pt) giving a total metal deposition of  $450 \text{ nm}$  (top surface).

Dice exposed to the sputter metal deposition process contained electrical shorts on all of the PSS devices. I-V testing of every PSS devices showed a  $200 \Omega$  short between power and ground where typical measurements identify it as being open. The location of these shorts were

identified using a technique known as Thermally-Induced Voltage Alteration (TIVA), a failure analysis technique using a laser scanning optical microscope equipped with a 1064 nm laser. The PSS device is connected to power and ground through microprobers connected to a Keithly 238 power supply. The power supply is kept at a constant current (1  $\mu\text{A}$  for this analysis) while the 1064 nm laser scans the PSS device. The laser will locally heat the scanned region. In the case of a short, the localized heating will produce a corresponding change in resistance associated with the shorted area. This resistance change (with the power supply kept at constant current) will result in a voltage fluctuation to maintain the constant current. It is these changes in power supply demands that are imaged as a function of the laser scanning position producing the TIVA image. Results of these findings identified the location of the shorts on the PSS devices and are shown in Figure 3-3. Arrows in both the reflected light image and TIVA image denote regions of interest where shorting occurs.

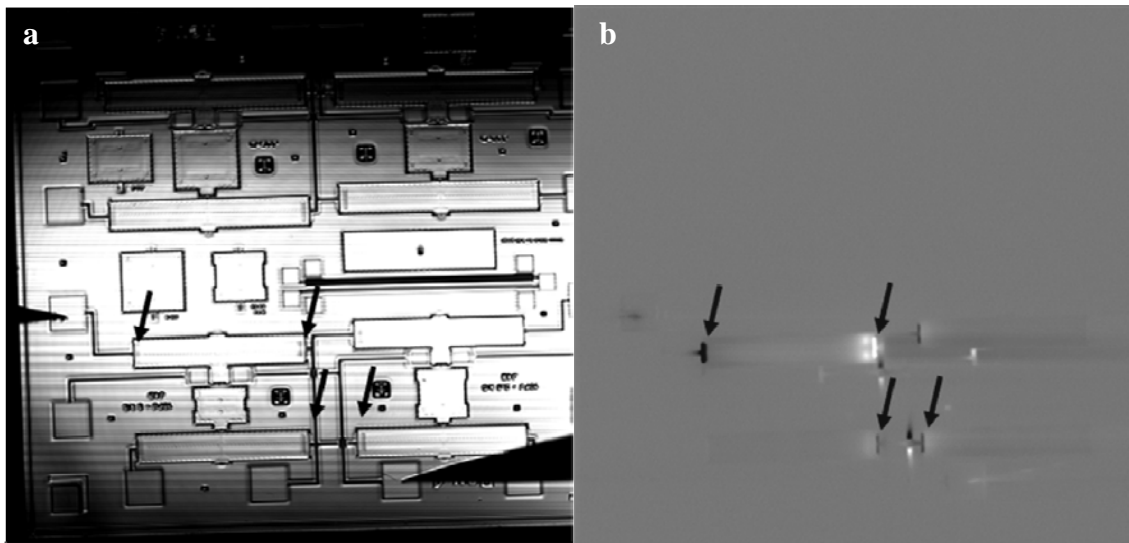


**Figure 3-3. a) Reflected light image of a PSS device post metal deposition, b) TIVA image using a 1064 nm laser with 1  $\mu\text{A}$  applied bias. Note the arrows identify sites of interest where an electrical short exists.**

SEM analysis of these TIVA sites did not reveal any particles, metal stringers or other gross metal defects contributing to a short. However, at high tilt angle, it appears the poly 4 cover layer does not extend out far enough to sufficiently mask the underlying polysilicon structures (such as poly 0) to prevent the metal from depositing on them during deposition. These results are shown in Figure 3-4 where high-angle SEM images of a thermal actuator show metal on the sidewall of the poly 4 cover as well as metal contacting the poly 0 layer underneath. The metal penetrating underneath the poly 4 cap contacting the poly 0 layer led to the short identified in all the thermal actuators on these dice from this metal deposition process. The degree of metal penetration underneath the poly 4 cap was also studied, but clearly the penetration of metal underneath poly 4 is significantly more than anticipated in this metal deposition process.

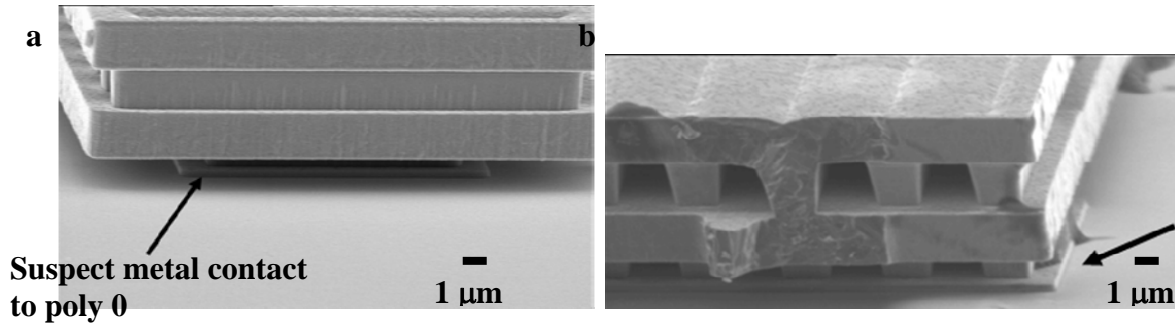


**Figure 3-4. a) SEM analysis of a thermal actuator edge does not shadow the underlying poly 0 structure indicating metal is contacting poly 0, b) metal contact confirmed on the right portion of the image. Note the dark contrast on the bottom of the left side (absence of metal) and the bright contrast on the right side (presence of metal).**

To verify the metal deposition extends deeper beneath the poly 4 cover, a cover from a PSS test structure was removed to expose the underlying proof mass and other polysilicon structures. Results of the metal deposition revealed the metal deposition extended  $\sim 17 \mu\text{m}$  underneath the poly 4 cover, significantly further than expected. In some instances, the penetration underneath the poly 4 cap is enough to reach the moveable shuttle as shown in Figure 3-5.

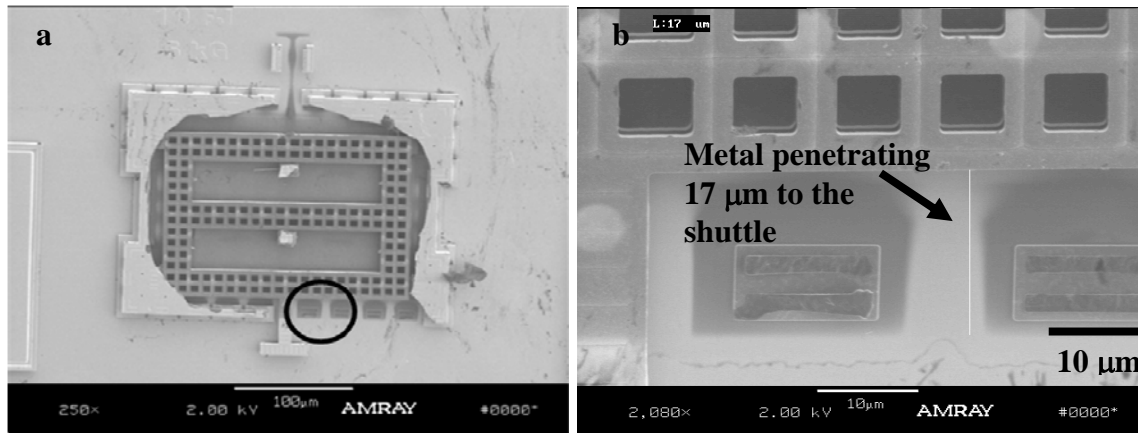


**Figure 3-5. a) SEM image of a poly 4 cover removed exposing a moveable shuttle, b) SEM image measuring  $17 \mu\text{m}$  of metal penetration underneath the poly 4 cover.**

The results of these failure analysis investigations led to modifications in the sputter metal deposition process and may result in slight modification of the poly 4 cover design to ensure adequate coverage of poly 0 ground planes and other electrically active structures during metal deposition.

To ensure metal thickness uniformity, SEM analysis was performed to measure the top and sidewall metal thickness. The target thickness for the top surface was  $\sim 425 \text{ nm}$ . A target thickness for the sidewall metal was not determined. A top level thickness of  $\sim 433 \text{ nm}$  was measured indicating the total thickness of Ti and Pt was on target to within 2%. Cross-sectional images of bond pad edges were taken to show the metal thickness of both top and side wall surfaces. As shown in Figure 3-6, the thickness measurements taken on the top and sides of a cross-sectioned bond pad measured  $192 \text{ nm}$  at the top and  $245 \text{ nm}$  sidewall thickness was expected

but until this time was not quantified. The contacts are exposed to the same metal deposition process and have the same metal thicknesses.

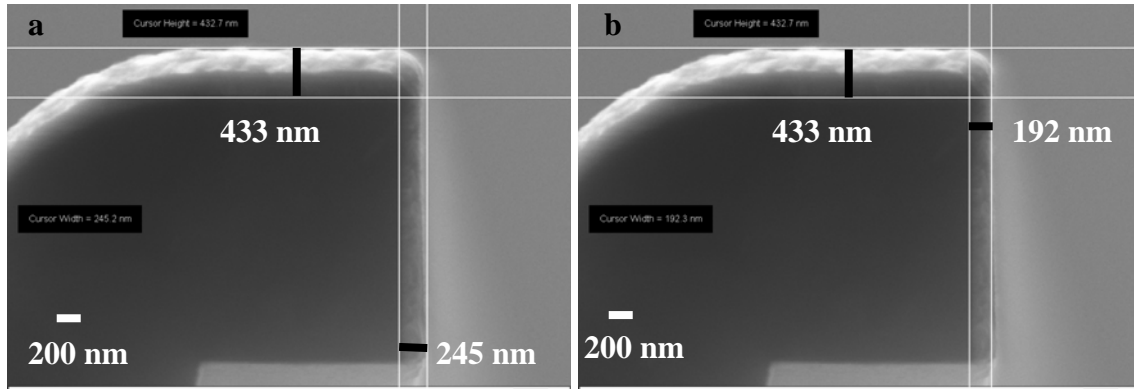


**Figure 3-6. a) SEM image showing Ti and Pt metal thickness on the top and side of a bond pad. Sidewall thickness measurement was taken at the bottom. b) SEM image with same thickness measurements but at a different location on the sidewall.**

### 3.1.3 Thick Polysilicon Process Development

Various fabrication runs were developed to create a thicker polysilicon stacked structure for the proof mass. These runs consisted of tying poly 1, 2, and 3 together, creating a 7.5  $\mu\text{m}$  thick structure. After releasing dice containing test structures with moveable shuttles, electrical stimulus identified no movement. After electrical stimulus, the probes were applied to the extended portion of the mass to move the shuttle. The shuttles were unable to move indicating that whatever was causing them to stick was very strong. As shown in Figure 3-7, the optical image shows a stuck moveable mass in a test structure while the infrared (IR) images through the poly 4 cover (not metalized) reveal small spots inside the etch release holes of the shuttle.

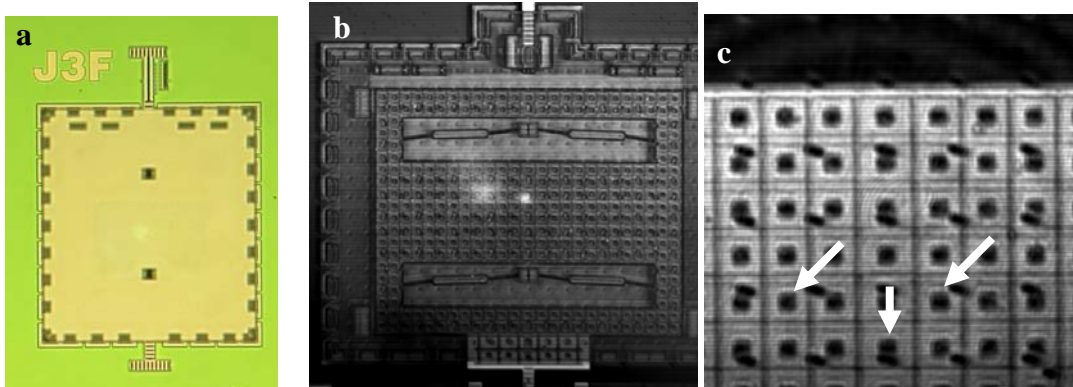


**Figure 3-7. a) Optical image of a released thick poly test structure, b) IR image of a released moveable shuttle, c) small dark spots are observed inside the etch release holes of the moveable shuttle (arrows).**

To examine the small spots further, the poly 4 cover was removed from one of the test structures. Removal of the poly 4 cover exposed several unexpected structures contained in nearly every etch release hole on the shuttle. Optical and SEM analysis confirmed they were present inside

each etch release hole. Energy dispersive x-ray analysis (EDS) taken on three of these unexpected structures confirmed the particles were silicon in origin. These structures are shown in Figure 3-8.

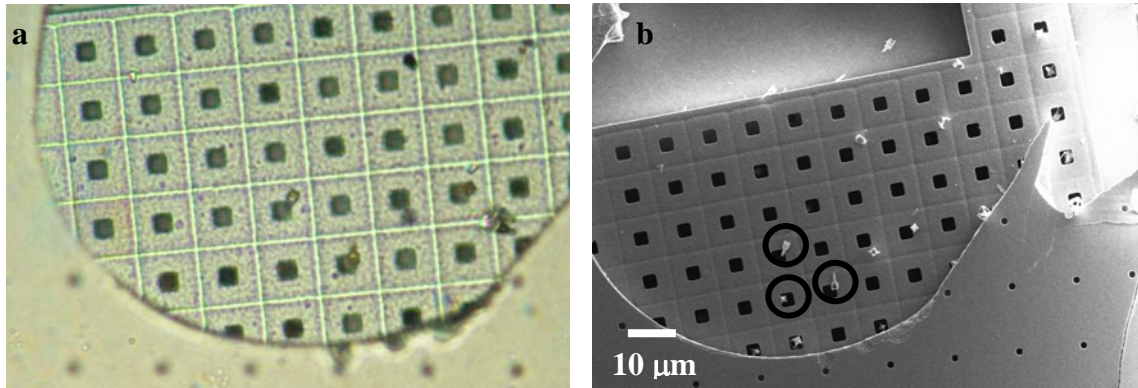


**Figure 3-8. a) Optical image of a moveable shuttle with the poly 4 cover removed (note the small particles in proximity to the etch release holes), b) SEM of the same area showing the structures in better detail (circle denotes EDS sample area).**

Higher magnification of the small structures shows “key-hole” defects. A released form of this defect and its corresponding EDS spectra are shown in Figure 3-9. The sacrificial oxide deposited into ordinary etch release holes in the SUMMiT process is sufficient to completely fill the hole prior to deposition of the next layer. However, in this design, the oxide did not fill the hole, leaving voids filled with polysilicon during the deposition process. This was verified using the FIB to cross-section an etch release hole in the shuttle on an unreleased part. The results from these analyses are shown in Figure 3-10. Note the failure occurred as the result of the polysilicon structure hanging from the bottom of the poly 4 cap as a “stalactite”. This structure was solidly attached to the poly 4 cap, preventing the shuttle from moving during electrical or mechanical stimulus.

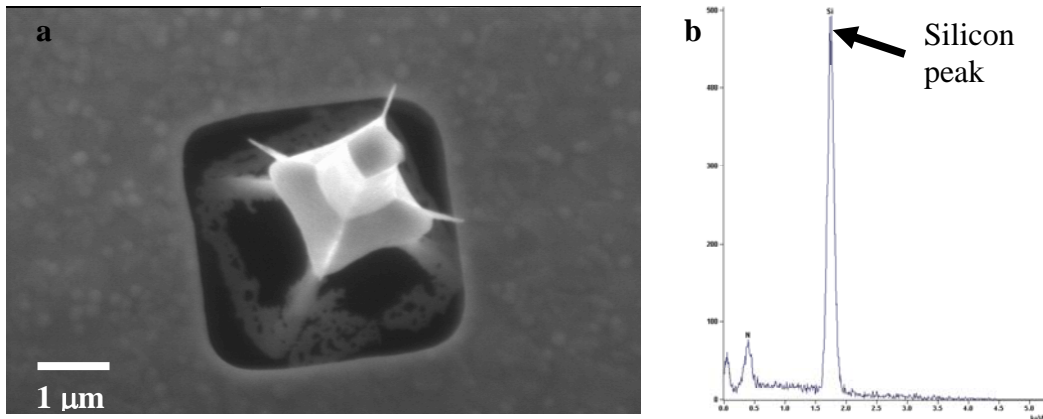


**Figure 3-9. a) SEM image of the material found in an etch release hole, b) its corresponding EDS spectra indicating the particle is silicon.**

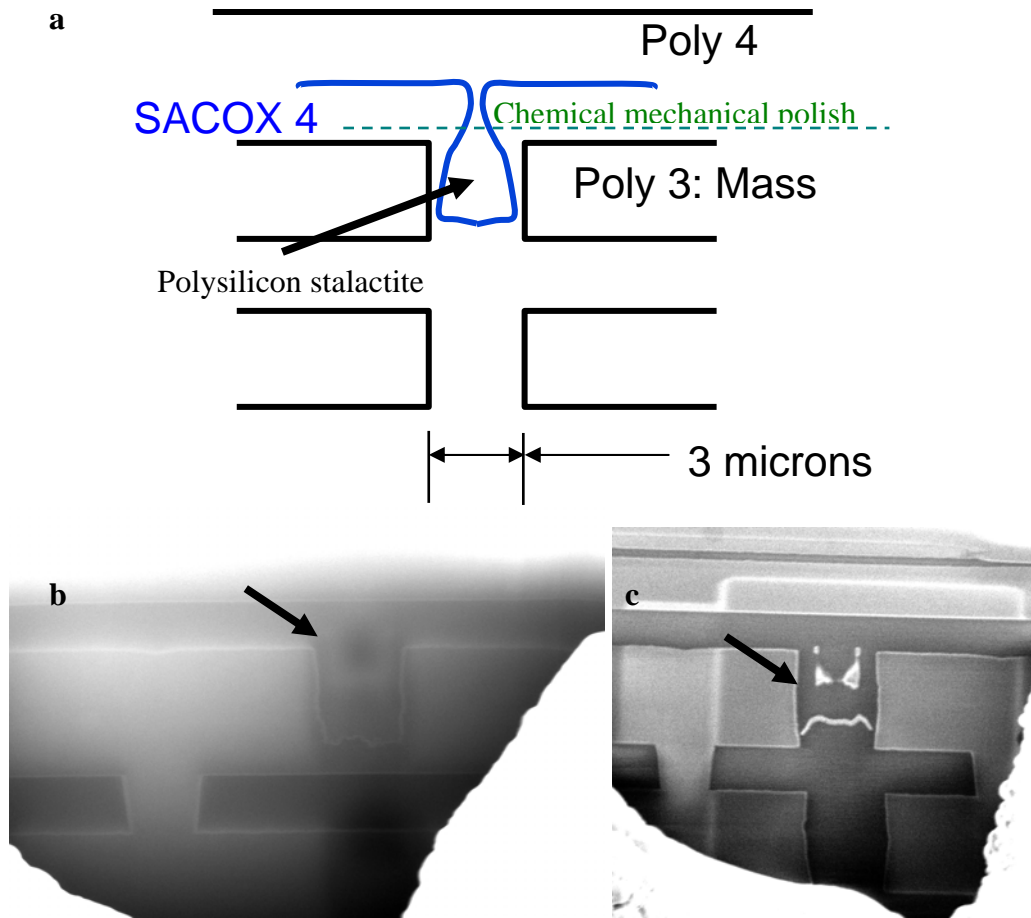


**Figure 3-10. a) Schematic cross-section illustrating key-hole defect, b) cross-section partially through the etch release hole (note the presence of the structure), and c) a cross-section  $\sim \frac{3}{4}$  through an etch release hole in the moveable shuttle showing the formation of the silicon “stalactite.”**

### 3.1.4 Silicon Nitride Isolation Process Development

In an effort to electrically isolate various regions of the PSS device, various dimple cuts were made and backfilled with silicon nitride. Revision 3 of the MEMS dice utilizes an isolating nitride layer to prevent the alternate current path discussed in [3]. The nitride backfill was designed using dimple cuts that are traditionally backfilled with polysilicon. In this case, dimple cuts were backfilled with silicon nitride creating silicon nitride anchors. These nitride backfilled anchors mechanically connect poly 1 and 2 to poly 3. A micro-tensile test structure designed with these nitride-based anchors is shown in Figure 3-11 along with a schematic illustrating the electrical isolation. In these structures, the nitride cuts vary in length. The objective of the test was to identify a failure site, not gauge the stress and strain required to induce failure or determine the level of electrical isolation provided by the nitride cut.

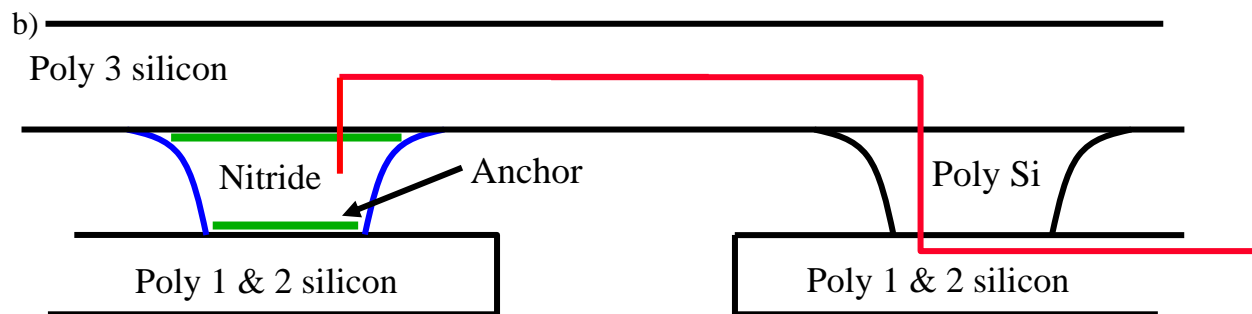
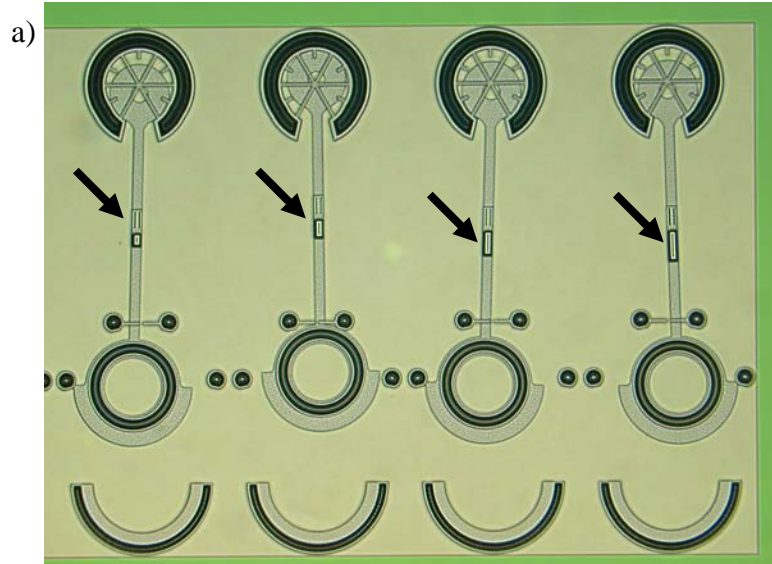


**Figure 3-11. a) Nitride isolation dimple cuts on tensile test structures. Arrows indicate the nitride dimple cut and backfill; b) Schematic of nitride isolation anchors which mechanical tie Poly 1 & 2 to Poly 3 (red line indicates electrical path isolation of left Poly 1 & 2 from Poly 3).**

To test the mechanical robustness of the nitride anchor, a probe was placed inside the ring and pulled, putting the test structure in tension. This force was applied until failure. No measurements were taken as to the stress and strain exerted on the sample at the point of failure. After failure occurred, optical and SEM examination of the fractured surfaces were performed to identify the point of fracture. These analyses showed failure typically occurred along the nitride/polysilicon interface. One sample failed via fracture along the polysilicon. The results of these pull tests are shown in the optical images of Figure 3-12.

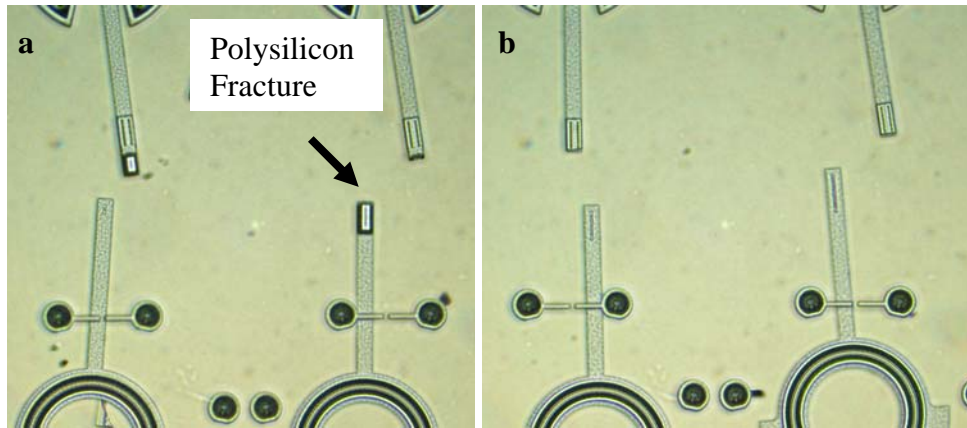


**Figure 3-12. a & b), Optical images showing the results of a pull test on the nitride isolation structures. Note only one sample failed at the polysilicon whereas the rest failed along the silicon nitride/polysilicon interface.**

Using an SEM, closer examination of the fracture surfaces on all four test structures identified unique features on the fracture surface. As shown in Figure 3-13, the failed samples appear to show polysilicon delamination between Poly 1 & 2 and the silicon nitride. In many cases, the delamination appears “clean” indicating that the failure was along the nitride/polysilicon interface with little or no removal of underlying material. In some instances, small polysilicon crystals were broken and or removed from the poly 1 & 2 layer at the interface. These can be seen in SEM micrographs in Figure 3-14. This evidence shows that for this particular anchor design failure first occurs at the nitride/polysilicon interface.

It can also be inferred that these structures are electrically isolated. Using an SEM, examination of these structures showed considerable charging on the polysilicon 1 & 2 layer. Charging occurs when the electrons injected into the polysilicon do not have a path to ground or are otherwise neutralized during imaging. In these cases, the “conductive” components (the top layer of polysilicon in this case) begin to charge during scanning, creating a “streak” around the structure during the scan. This is observed in Figure 3-13 b and Figure 3-14 b. Although it is not a direct electrical measurement as to the resistivity of the nitride cut, the occurrence of charging strongly indicates electrical isolation from one structural element to another.

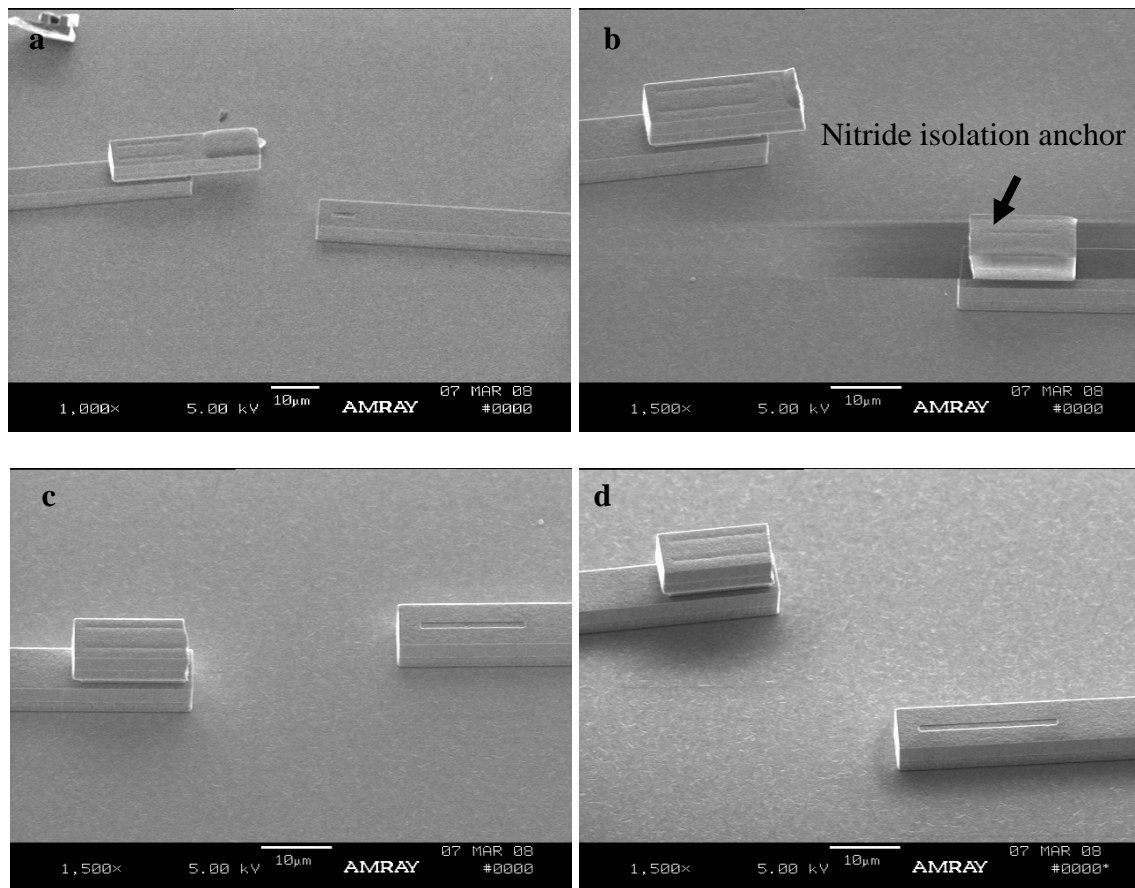


**Figure 3-13. Fracture surfaces of test structures with silicon nitride isolation a) failure at the silicon nitride/poly interface, streaking b) fracture on the polysilicon layer, c & d) failure at the silicon nitride/poly interface.**

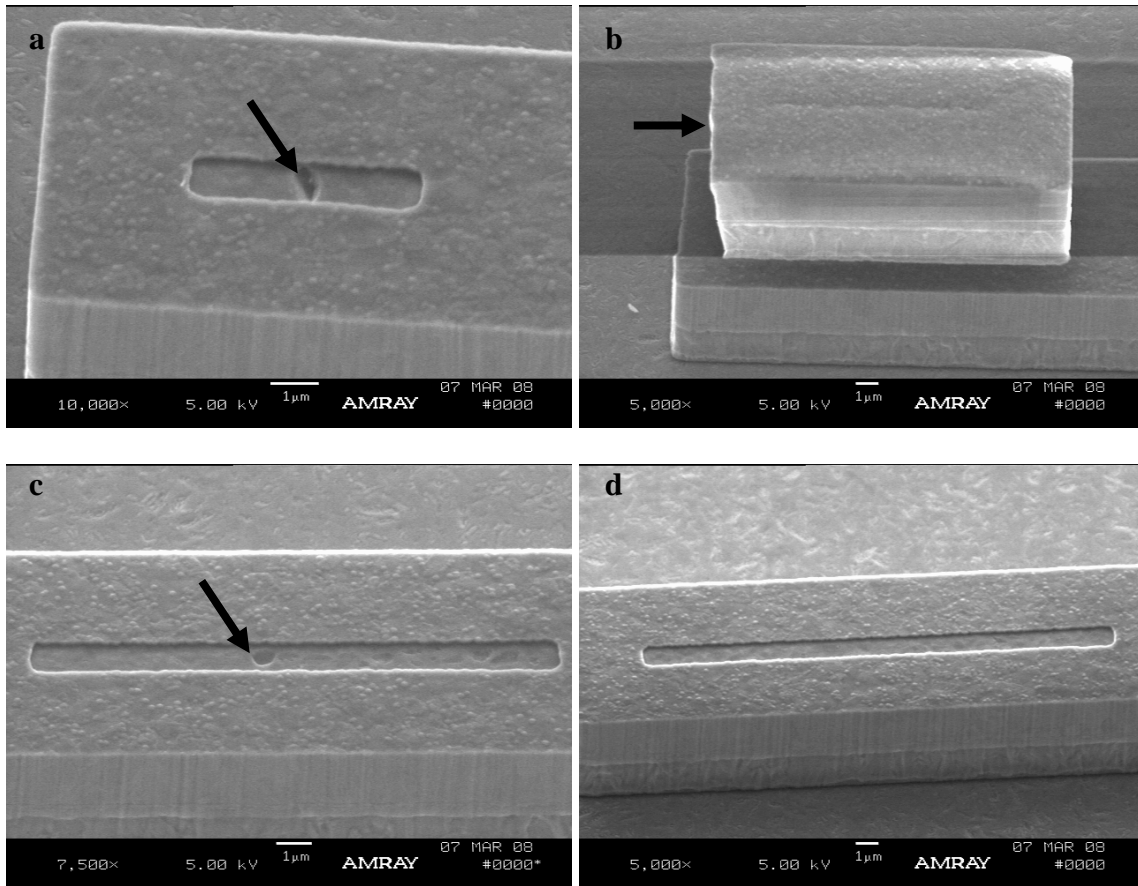


**Figure 3-14. a) Short nitride isolation cut interface with a small polysilicon grain missing indicating polysilicon delamination, b) fracture of the polysilicon with the nitride still adhered to the poly, streaking; c) nitride delamination on a 15  $\mu\text{m}$  long isolation cut (note the extruded grains), and d), nitride delamination.**

### 3.2 Passive Shock Switch Failure Analysis: Package Level

Failure analysis activities for PSS packaged parts were performed on devices subjected to self-testing, shock, and thermal testing. In the self-test, PSS devices are subjected to electrical stimuli to place the PSS component in the closed position, then stimulated again to place it in the open position. This test was performed 2 – 4 times to verify the switch is capable of opening and closing repeatedly. In the shock test, PSS devices were subjected to different shock loads designed to close the switch. In the thermal test, PSS components are subjected to a constant thermal stress. In this test, the PSS components are in the open position. The failed devices from these tests were compared to functional devices for accurate assessment. In several instances, the failures from both tests appeared to be either stuck closed, stuck open or intermittent (temporarily stuck open or temporarily stuck closed). More information regarding the self-test, shock test, and thermal test can be found in reference [4].

### 3.2.1 Self-Test and Shock Test

The self-test is performed as a “self-assessment” or assessment of device functionality by providing an electrical stimulus to set the PSS in the open or closed state. Failures observed from self-tests include; the PSS is stuck open (inability to close with applied electrical stimulus) and stuck closed (inability to open with applied electrical stimulus). Shock tests were performed to ensure the PSS devices closed at the appropriate rated shock level. PSS devices were defined as failing if they were unable to detect shock due to contacts being stuck open or closed.

Several methods were used to aid in localizing the failure site and diagnosing the root cause of failure. For board-level and packaged parts, electrical analysis identified the parts that required further analysis. After the failure was verified, a small razor blade, a hammer, and a vice were used to stabilize the packaged part and remove the lid from the solder ring. This lid removal process allowed the failure analyst to gain access to the die for static and dynamic visual inspection. This process is shown in Figure 3-15 a-c.

The packaged part is held in the vice and clamped tight enough to hold the part snug. A set of protection goggles or glasses are worn while positioning the utility razor at the corner of the lid and solder ring. While the razor blade is held in place, the hammer is used to gently tap the razor blade between the package lid and the solder ring. Extra care should be taken to position the packaged part such that any particles generated during the delidding process will fall out and away from the die and the active elements. Once the lid is removed, the PSS devices are exposed and ready for structural analysis in either static or dynamic conditions. By reducing particulate contamination and exercising care during the delidding process, the part is still electrically functional and can be stimulated under an optical microscope.

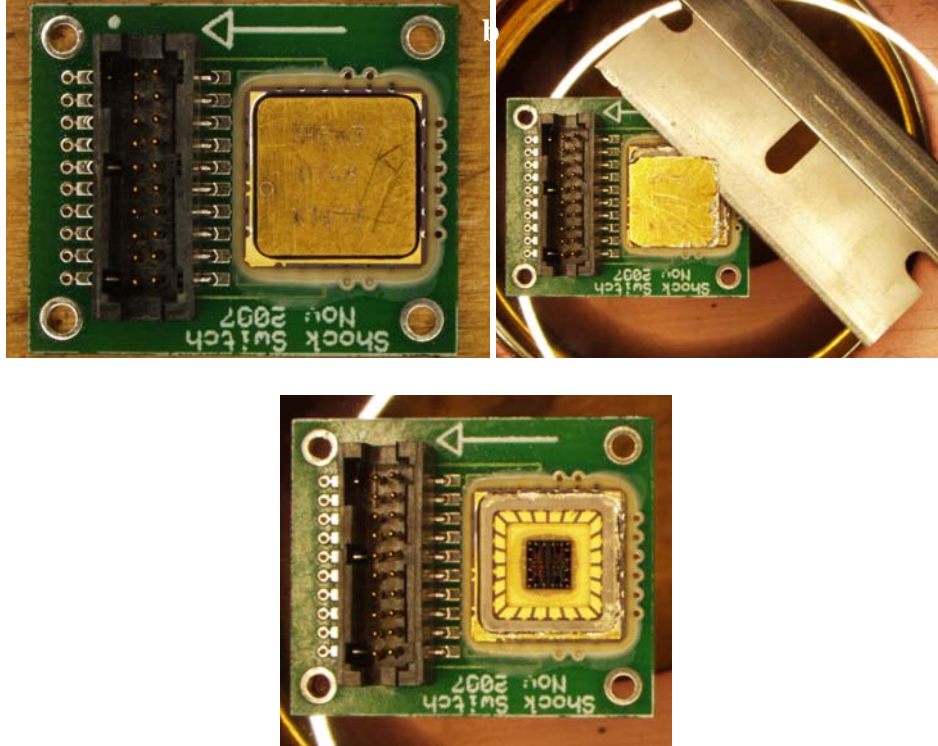


**Figure 3-15. Delidding procedure demonstrated on a) PSS mounted on a board, b) razor blade perforating the seal along the lid/solder ring, and c) lid removed exposing the die.**

In static inspection, the part was characterized using both optical and scanning electron microscopy, checking for any gross structural irregularities or damage associated with the failing part. All elements of the PSS device were investigated. Emphasis was placed on those elements of the device that contain contacting or rubbing surfaces.

For switches that were stuck open, no irregular features or damage was identified. Visually devices stuck closed are identified by observing the contact region and noting that the contact bar is touching the contacts. Typically no damage is associated with either stuck open or stuck closed failure modes. Optical images of PSS devices failing self-test are shown in Figure 3-16. Note the small particles observed on the substrate generated from the solder ring used to keep the lid in place are ignored as they are not part of the root cause of failure. Closer analysis of the contact bar and contacts on the stuck closed failures did not reveal adhesion, welding, or sticking of these regions as the cause of failure. Exposed metal surfaces were free from contaminants and lacked any discoloration or damage consistent with any type of sticking phenomena.

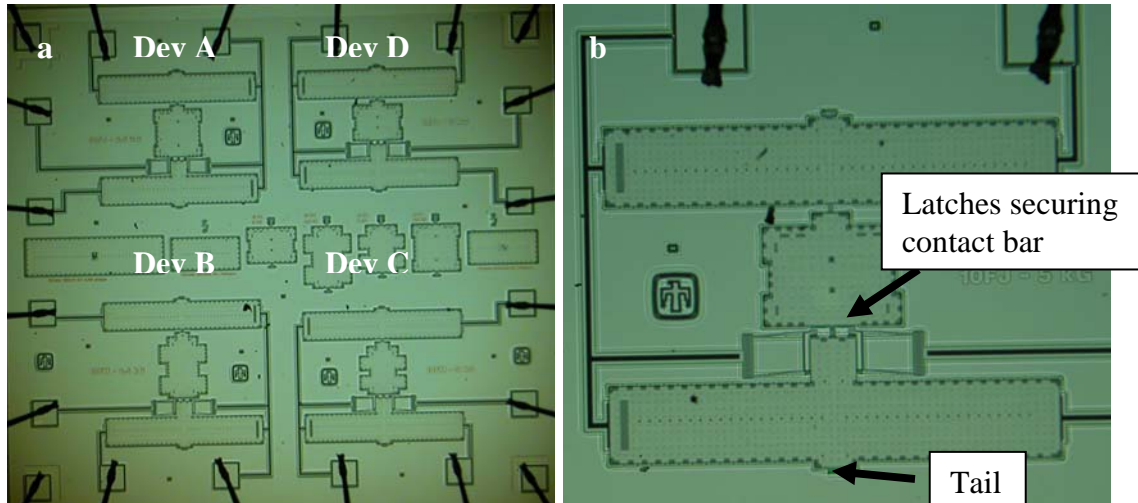


**Figure 3-16. a) Delidded and exposed die from self-test, b) close-up of device D.**

For dynamic visual inspection, the PSS device was operated under an optical microscope by providing the appropriate electrical stimulus. Dynamic analysis of the moving structures in their biased state gives the failure analyst information on the functional aspects of the device as well as a starting point to identify the root cause of failure. Each element of the device could be analyzed independently. As discussed earlier, the PSS device consists of 2 thermal actuators positioning a moveable, bi-stable mass into either an open or closed state. After the contact bar is latched and the bi-stable mass is in position, the mass moves either due to additional force from the thermal actuator or due to a shock load along the sense axis of the device [4].

For the PSS devices failing self-test and shock test, the thermal actuators functioned properly. Although hidden underneath the poly 4 cover, the thermal actuator movement could be analyzed by movement of the polysilicon tab or “tail” located just outside the poly 4 cover shown in Figure 3-16 b (bottom arrow). If the thermal actuator tails move their full range, we eliminate the thermal actuators as being the root cause of failure. When in the closed position, the contact bar can easily be analyzed. We also ensure the contact bar is appropriately latched by position of the springs on the left and right side of the switch (Figure 3-16 b, top arrow). After static and dynamic analysis of PSS devices from self-test, the actuators are functional. This suggests the problem lies in a different mechanical element of the PSS device, likely somewhere in the proof mass.

Since the moveable bi-stable mass is not easy to see during device operation, many different techniques were used to remove the poly 4 cover and examine the proof mass. These techniques included breaking the cover, removal of the top level Pt by FIB processing, removal of the Pt by acid, and other methods of removing the cover. The design of this cap shows 50 anchors around the perimeter, 4 just inside the perimeter, and 6 interior anchors connecting the poly 4 cover over the proof mass to the substrate.

Any technique involving breaking the poly 4 cover resulted in a number of polysilicon particles and often times, damage to the mass. Although this method proved useful for initial inspection, it would often result in compromising the failure mode and prevented further analysis. Etching

techniques such as wet chemical etch and FIB deprocessing to remove the top level Pt were unsuccessful. Wet etch chemistries designed to remove Pt wicked underneath the cover plate contacting the bi-stable mass and compromised the failure mode. FIB deprocessing techniques were designed to mill off the Pt from the poly 4 cover and expose the polysilicon for infra-red microscopy. IR techniques can be used to “see-through” the polysilicon and analyze the underlying structures. This deprocessing technique was successful in removing the Pt, but it created a rough surface causing too much light to be dispersed through the poly 4 cap. This significantly reduced the amount of information on structures underneath the cap. Plasma deprocessing techniques to remove Pt were not employed.

One approach that proved successful in removing the poly 4 cap with little to no damage to the bi-stable mass involved using the FIB in conjunction with an in-situ probe. The FIB was used to strategically cut a pattern around the poly 4 cover. For this process to be successful, FIB cuts were positioned around the interior of the anchors holding the poly 4 cover in place. Once the cuts were made, an in-situ probe was positioned on the cut portion of the cover. Once contact was made, a gas insertion system (GIS) containing Pt was brought in proximity to the probe and poly 4 cover. Pt was locally deposited onto the probe and poly 4 cover, “welding” the probe to the cover. After the “welding” process was performed, the probe and welded poly 4 cover were excised from the device, exposing the underlying bi-stable mass. Images detailing this process are shown in Figure 3-17.

After removing the poly 4 lid, structural analysis was performed on the underlying bi-stable mass. As shown in Figure 3-18, the poly 4 cover was removed with minimal damage to the bi-stable mass. After removing the poly 4 cover, several areas of interest were examined. The mass appears to be in good structural condition, even with minor FIB damage to the spring mechanisms. Initial inspection showed the mass is still positioned in the bi-stable state, consistent with the same position it was in prior to performing the FIB cuts. Inspection of the mass and surrounding structures did not reveal any wear debris, wear tracks, or other features consistent with rubbing or contact as shown in Figure 3-18. As no defects or debris was observed, the bi-stable mass was removed to expose the underlying substrate and other structures of interest.

After removal of the bi-stable mass, portions of the side structures located underneath the poly 4 cover anchors were analyzed. Results of these SEM analyses shown in Figure 3-19 (a & b) did not identify damage on the top surface of the bi-stable mass or the exposed bottom surface of the anchor to poly 4. Analysis of the design in this region (Figure 3-19 a, arrows) showed a poly 1 dimple in proximity to the anchor. This dimple on the bottom of the bi-stable mass and its mirror surface on the substrate were examined. Results from these analyses showed a higher level of contrast in circular region similar in geometry to the poly 1 dimple on the bi-stable mass. This region of different contrast may be indicative of contamination in that region as shown in Figure 3-20. Unfortunately, due to the method of lift-out used to extract the bi-stable mass (probe tip with adhesive tape), we cannot confirm at this time whether the spot observed in Figure 3-20 was caused by the lift-out process extraction or whether it occurred during the test. If other failures from shock testing become available, more analysis and alternate methods of extracting the bi-stable mass will be performed to identify the root cause of failure. However,

other samples from self-testing and thermal testing where the poly 4 lid and bi-stable mass were removed did not show the dark spots observed in the shock test.

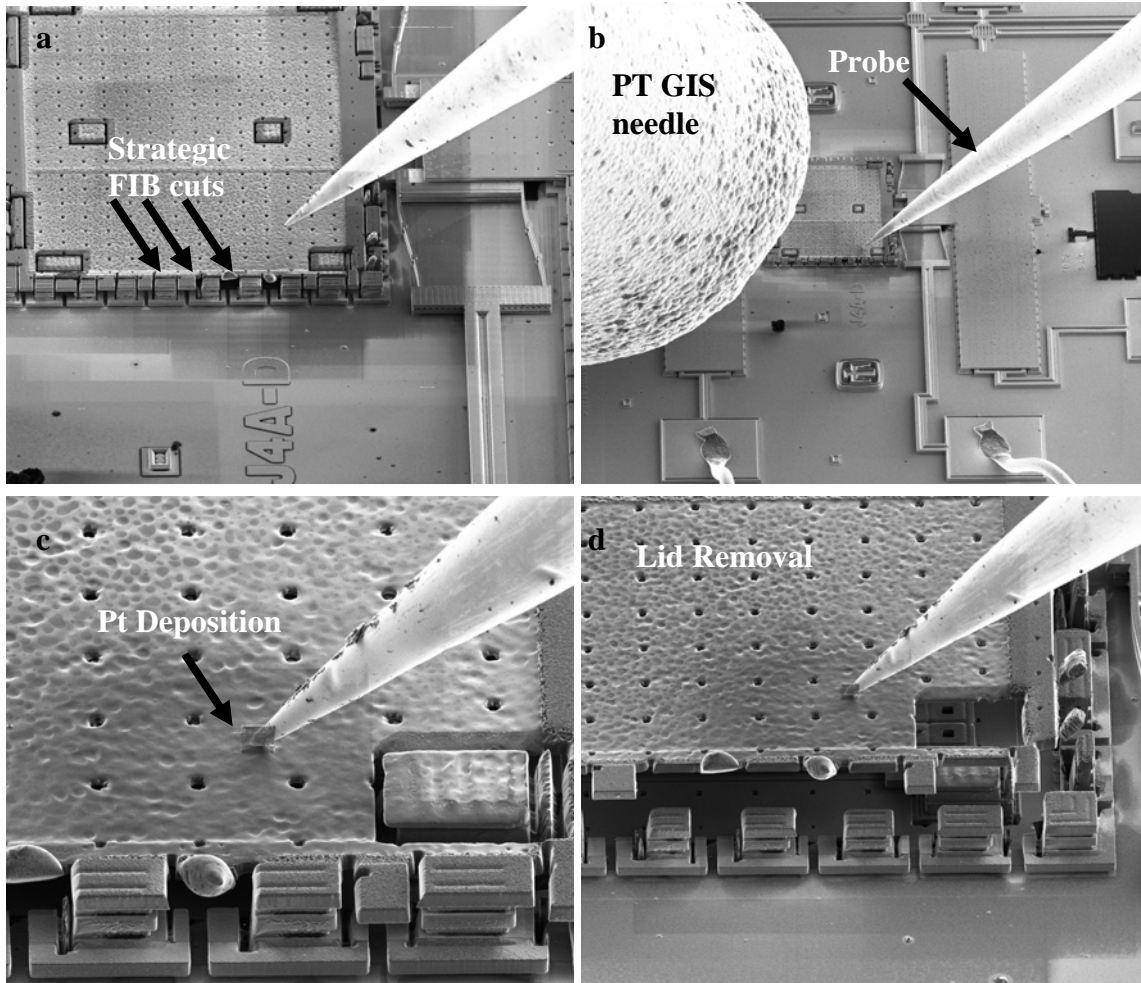


Figure 3-17. Poly 4 cover plate removal process by a) strategic FIB cut layout, b) Pt GIS insertion, c) Pt deposition, and d) lid removal. Lid removed on part X1043.

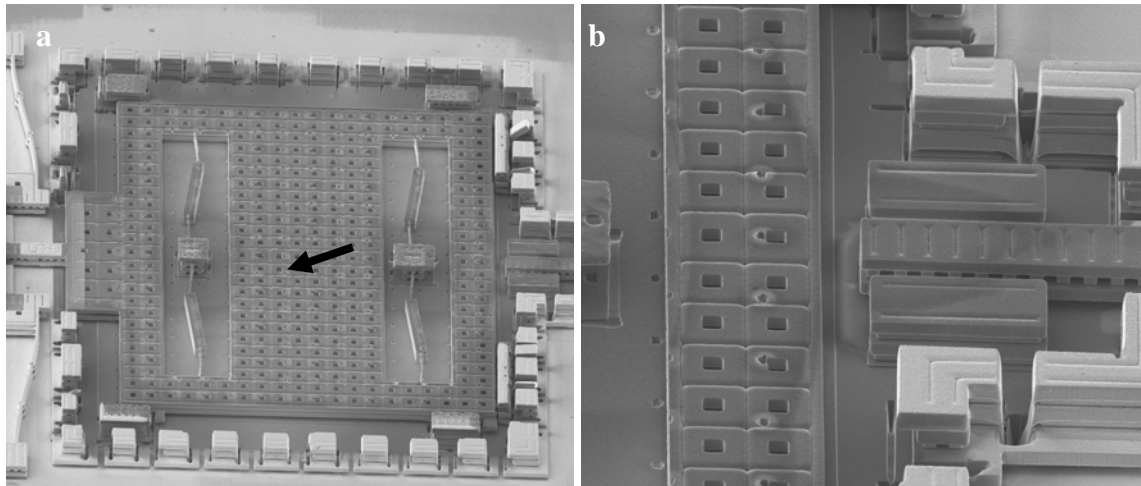


Figure 3-18. a) Poly 4 cover removed exposing the underlying proof mass, b) closer examination of the thermal actuator/proof mass contact.

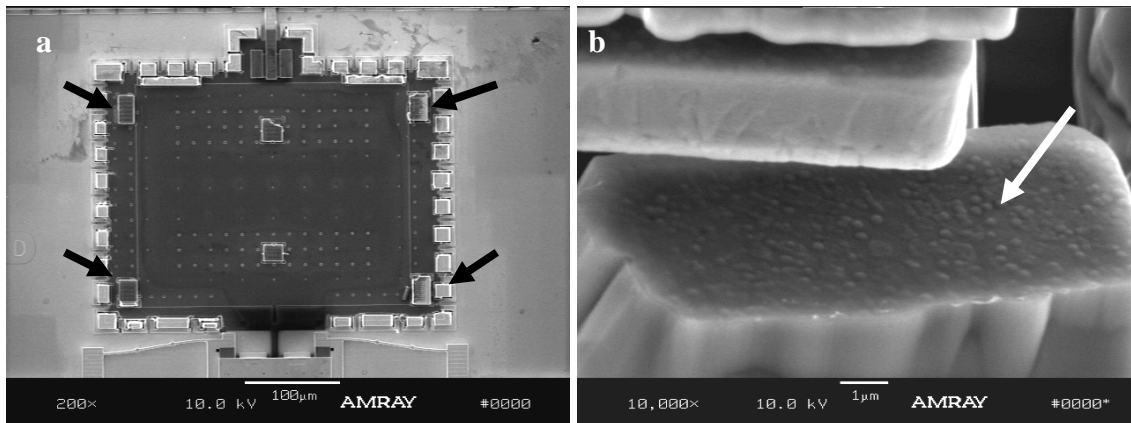


Figure 3-19. a) Bi-stable mass removed, exposing the underlying the substrate and anchors (arrows), b) SEM analysis of the portion of the polysilicon bi-stable mass underneath the anchors (arrow), no sign of damage, rubbing, or gouging was observed.

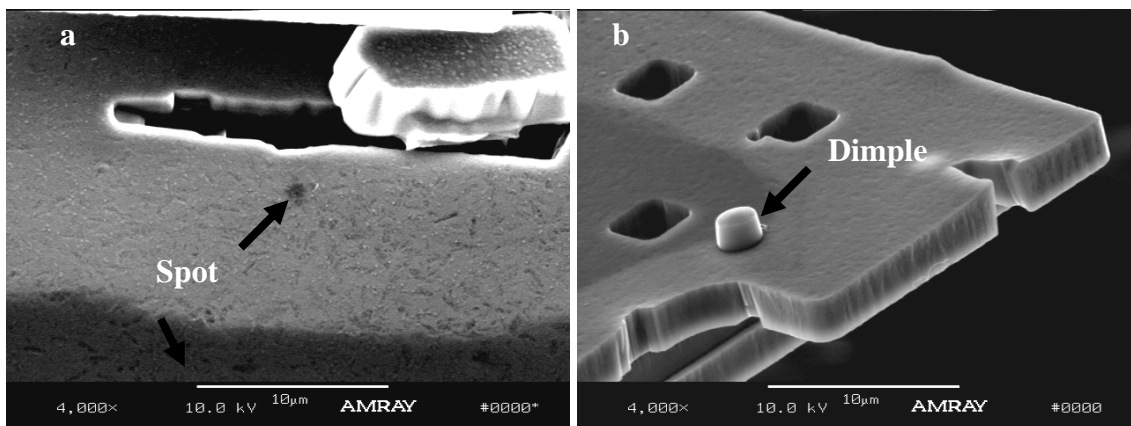
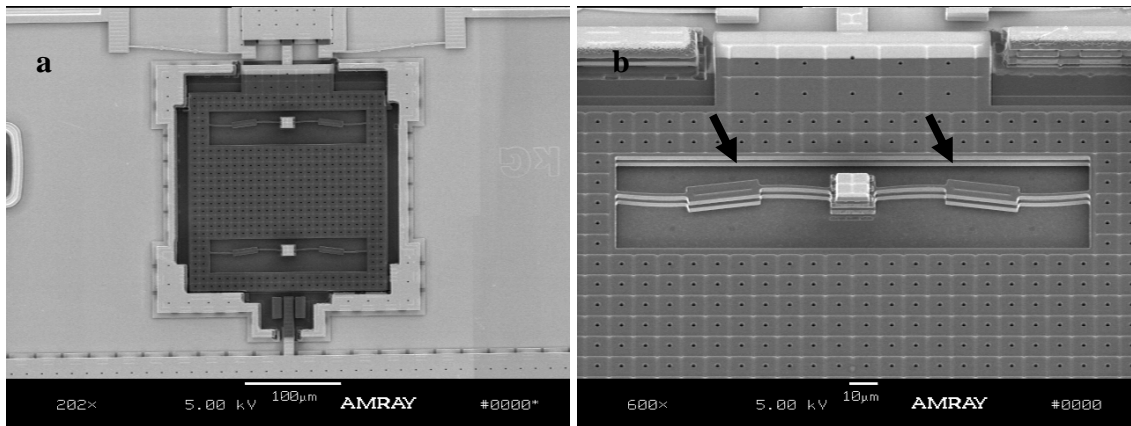
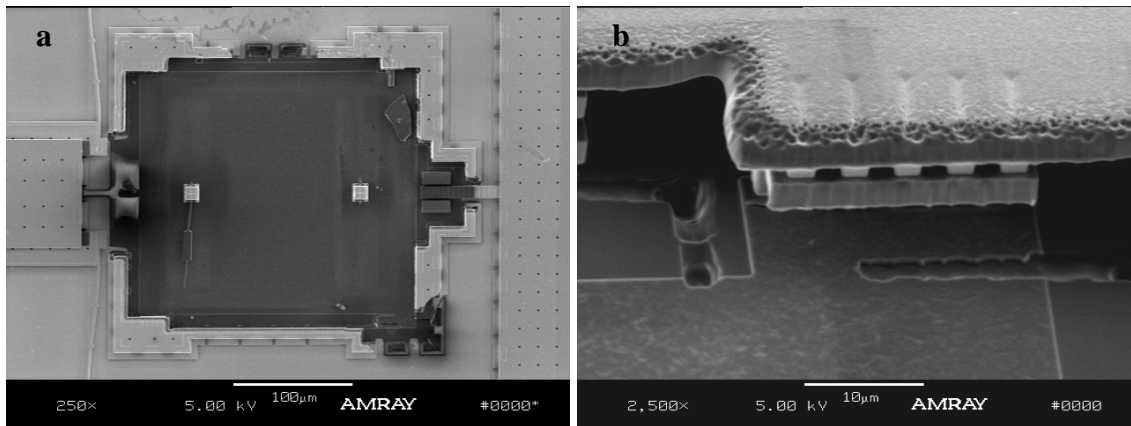


Figure 3-20. a) Possible contamination spot on the substrate coincident with the poly 1 dimple shown in b).

Sample X1031 failed self testing in a manner similar to the shock test sample. The same failure analysis methodology was used to examine this device with and without the poly 4 cap. Analysis of this device (not shown) did not aid in identifying the root cause of failure, but dynamic analysis indicated both thermal actuators operated correctly, indicating the problem lies somewhere within the bi-stable mass. As with the failed shock tested part, the poly 4 cover was removed for inspection and analysis. No obvious damage or structural degradation was observed and the device was still in the bi-stable position (as-received) after FIB deprocessing as shown in Figure 3-21. Analysis of the metal contacts did not show any contamination, welding or other defects. After removal of the poly 4 cover, the device was actuated and little to no movement was observed in the mass during operation. Failure analysis on self-test failed samples is ongoing. Also see Figure 3-22.



**Figure 3-21. a) Self-test sample X1031 with the poly 4 cover removed, and b) close-up view of the bi-stable mechanism.**



**Figure 3-22: a) Bi-stable mass removed exposing the substrate, and b) analysis near an anchor did not reveal any dark spots.**

### 3.2.2 Thermal Testing

Packaged PSS devices were subjected to a “normal environments” thermal test [10]. In these tests, the PSS device was in its opened position; no surfaces were in contact during thermal stress. After thermal testing, the PSS devices were stimulated using the self-test to determine

pass/fail. A failing device was defined as the inability of the PSS to complete a self-test (successful open and close cycle). Failing devices identified via self-test were given to failure analysis. After package inspection, the package lid was removed, exposing the PSS die. Inspection showed signs of contamination on the surface of the substrate and poly 4 covers. Slight discoloration was observed in bright field optical microscopy but in dark field, several contamination spots could be observed on top of the substrate and the poly 4 as shown in Figure 3-23. This device was also stimulated after lid removal and again, the thermal actuators functioned while the proof mass did not move. This result indicates the problem is contained somewhere inside the proof mass and is likely mechanical in nature. Electrical testing did not reveal any shorts preventing the device from moving. Analysis of the contacting surfaces did not reveal any welding, adhesion, or defects that would cause sticking as shown in Figure 3-24; therefore, the poly 4 cover was removed for more detailed analysis of the underlying bi-stable mass.

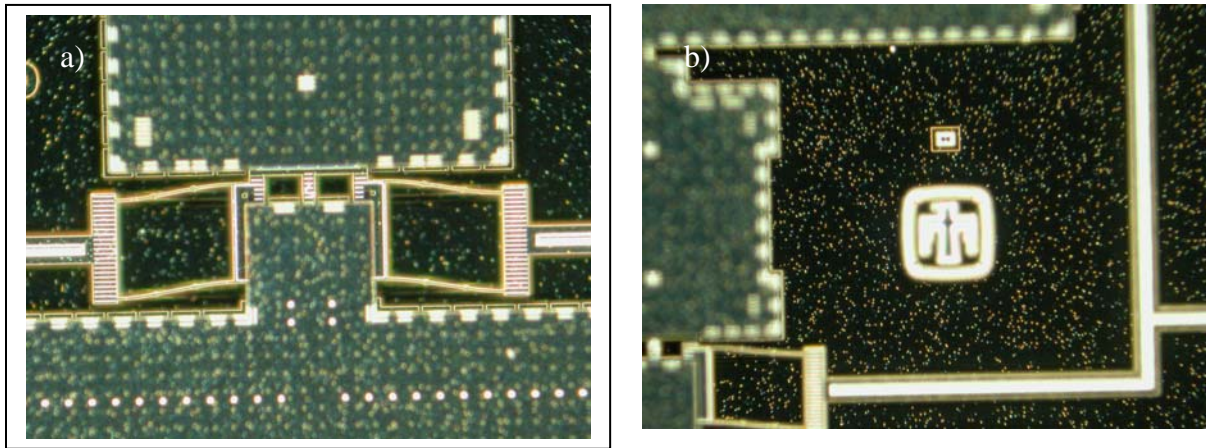


**Figure 3-23. a & b) Dark Field optical microscopy exposing contamination on the substrate of a thermally tested PSS component.**

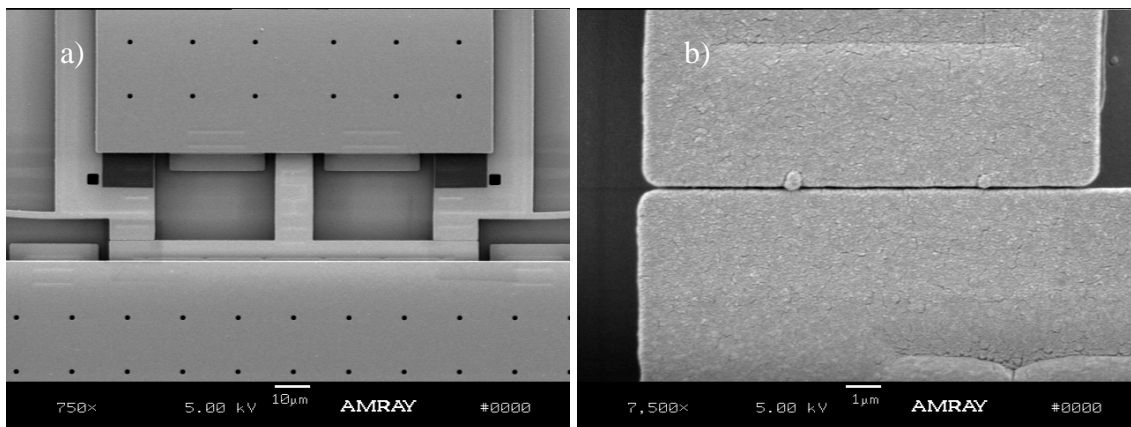


**Figure 3-24. a & b) SEM analysis of contacts did not reveal any welding or other defects.**

After the poly 4 cover was removed, the PSS device was tested to examine any potential sticking areas. This test showed the bi-stable mass did not move when pushed using the thermal actuator. Closer analysis did not show welding or damage leading to the root cause of failure, so the bi-

stable mass was removed to examine the underlying substrate. It was speculated that the contamination identified on the substrate and top surface of the exposed poly 4 may be diffusing underneath the cover and bi-stable mass. Removal of the poly 4 cover and the bi-stable mass revealed some material on the underlying substrate in proximity to an FIB deprocessed location, but no clear accumulation of material. As shown in Figure 3-25, the substrate underneath the bi-stable mass appears to have a small dark spot located in the same region as the poly 1 dimple on the bottom of the bi-stable mass. This dark contrast may be the result of contamination build up bridging the substrate to the poly 1 dimple. In many cases, when devices fail self-test, slightly higher voltage applied to the thermal actuators results in more force and displacement. This additional force is often sufficient to “free-up” a stuck bi-stable mass from its failing position. Although the evidence is not conclusive at this time, we believe these dark spots represent areas of contamination accumulation that bridge up to the poly 1 dimple. This “sticking” creates additional friction and may or may not prevent the PSS device from operating correctly. We speculate this may be occurring at this time. More failed samples are needed to validate the theory and additional devices are needed to perfect the poly 4 cover removal and bi-stable mass removal process.

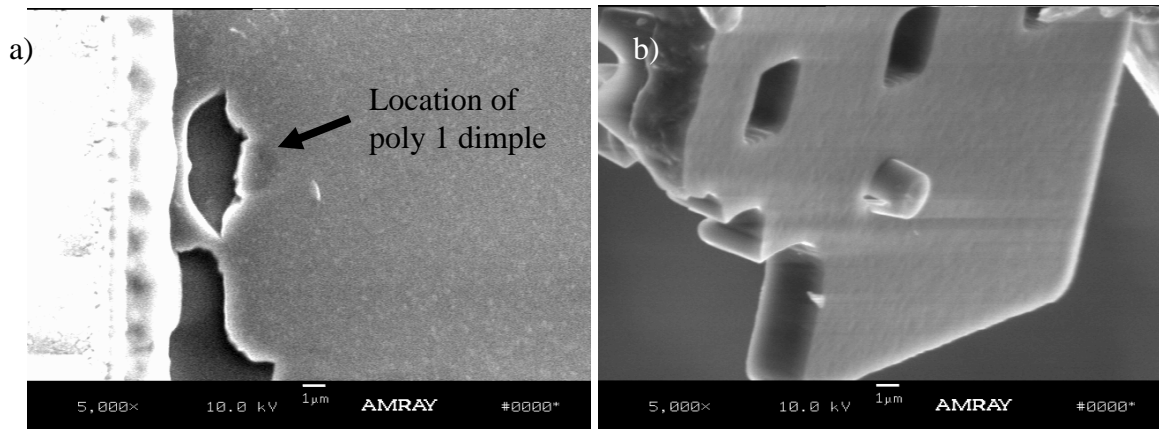


**Figure 3-25. a) SEM image of the poly 0 substrate underneath the bi-stable mass showing a small dark spot coincident with the poly 1 dimple location, b) poly 1 dimple on the bottom of the bi-stable mass.**

## 4. Conclusions

Failure Analysis has provided valuable insight into many of the failure mechanisms observed during fabrication, manufacturing and testing of PSS devices. Outside of fabrication anomalies, preliminary evidence shows there may be contact of poly 1 dimples with the substrate creating friction and possibly sticking. More analysis on failed samples is needed to validate this theory.

Previous methods used to remove the poly 4 cap and excise the bi-stable mass were more destructive to the device and often compromised the failure mechanism. A new method for removing the poly 4 cover enables direct observation of the proof mass in both a static and dynamic state. After this analysis is performed, the bi-stable mass can be removed with minimal damage to important structures and “preserving” the root cause of failure. Now that this technique has been developed, future failure analysis activities on PSS devices will employ this new cover and mass removal method to facilitate root cause failure analysis of packaged, “stuck” PSS devices.



## 5. References

- [1] J.A. Mitchell, J.W. Wittwer, M.S. Baker, N. Spencer, K.P. Pohl, R.C. Clemens, D.S. Epp, J.C. Gilkey, L.M. Phinney, W. Wilbanks, W.Y. Lu, *On the Design, Packaging and Testing of Micro- and Meso-scale Inertial G-Relays*, SAND2006-5806. Sandia National Laboratories, Albuquerque, NM, 2006.
- [2] M.S. Baker, C. Gustafson, M. Girardi, R.W. Schroeder, R.L. Hamm, B.D. Young, R.J. Brown, J.T. Slanina, F. Olivias, J.R. Dokos, R.C. Clemens, J.A. Mitchell, M.R. Brake, J.W. Wittwer, D.S. Epp, J.A. Walraven, *Packaging the MEMS Passive Shock Sensor*, (to be submitted as a SAND report in 2008), Sandia National Laboratories, Albuquerque, NM, 2008.
- [3] J.A. Mitchell, M.S. Baker, R. Clemens, D.S. Epp, J.A. Walraven, and J.W. Wittwer *Summary Report on the MEMS and MESO-scale Passive Shock Sensors Developed under the Embedded Evaluation Program FY07*, October 2007.
- [4] J.A. Mitchell, M.S. Baker, J. Blecke, R.C. Clemens, D.A. Crowson, D.S. Epp, J.E. Houston, J.A. Walraven, J.W. Wittwer, *The Sandia MEMS Passive Shock Sensor: FY07 Maturation Activities*, SAND2008-5184, Sandia National Laboratories, Albuquerque, NM, 2008.
- [5] E.I. Cole Jr., P. Tangyonyong, D.A. Benson, and D.L. Barton, TIVA and SEI Developments for Enhanced Front and Backside Interconnection Failure Analysis, in *ESREF*, pp. 991-996, 1999.
- [6] E.I. Cole Jr. and R.E. Anderson, Rapid localization of IC open conductors using charge-induced voltage alteration (CIVA), in *IRPS*, pp 288-298, 1992.
- [7] E.I. Cole Jr., J.M Soden, J.L. Rife, D.L. Barton, and C.L. Henderson, Novel failure analysis techniques using photon probing in a scanning optical microscope, in *IRPS*, pp. 388 – 398, 1994.
- [8] E.I. Cole Jr., Beam-Based Defect Localization Methods, in *Microelectronics Failure Analysis Desk Reference*, 5<sup>th</sup> Ed., pp. 406 – 416. ASM International, Materials Park, OH, 2004.
- [9] J.A. Walraven, E.I. Cole Jr., and P. Tangyonyong, Failure Analysis of MEMS Using Thermally-Induced Voltage Alteration,” in *Proceedings from the 26<sup>th</sup> International Symposium on Testing and Failure Analysis*, pp. 489 – 496, Nov. 2000.
- [10] D.S. Epp, J. Blecke, M.S. Baker, R.C. Clemens, M.R. Brake, J.A. Mitchell, J.A. Walraven, J.W. Wittwer, *Testing and Characterization of the MEMS based Passive Shock Sensor*, (to be submitted as a SAND report in 2008), Sandia National Laboratories, Albuquerque, NM, 2008.



## Distribution

1	MS0340	John L. Sichler, 2123
1	MS0340	Steve Harris, 2123
1	MS0343	Mary E. Gonzales, 2120
1	MS0344	George Clark, 2626
1	MS0372	James M. Redmond, 1525
1	MS0421	Michael R. Sjulín, 0240
1	MS0427	Robert A. Paulsen, 2011
1	MS0447	Matt Kerschen, 2111
1	MS0530	Hae-Jung L. Murphy, 2623
1	MS0633	Todd Sterk, 2952
1	MS0824	Tze Y. Chu, 1500
1	MS0847	Peter J. Wilson, 1520
1	MS1064	Joel B. Wirth, 2614
1	MS1064	Rebecca C. Clemens, 2614
1	MS1064	Ernest J. Garcia, 2614
1	MS1064	Marc A. Polosky, 2614
4	MS1064	John A. Mitchell, 2614
1	MS1069	Mark R. Platzbecker, 1749-1
1	MS1069	Michael S. Baker, 1749-1
1	MS1069	Danelle M. Tanner, 1749-1
1	MS1069	Jonathan W. Wittwer, 1749-1
1	MS1070	Channy C. Wong, 1526
1	MS1070	Jill Blecke, 1526
1	MS1070	David S. Epp, 1526
1	MS1080	Keith Ortiz, 1749
1	MS1081	David J. Stein, 1726
1	MS1081	Jeremy A. Walraven, 1726
1	MS1160	Douglas A. Dederman, 5431
1	MS1415	David R. Sandison, 1110
1	MS1415	Carlos Gutierrez, 1114
1	MS1415	Douglas A. Crowson, 1114
1	MS1415	Jack E. Houston, 1114
1	MS9042	Davina M. Kwon, 8770
1	MS9102	James F. Stamps, 8235
1	MS9102	Paul Y. Yoon, 8235
1	MS9153	Russell G. Miller, 8240
1	MS9154	Janson Wu, 8244
1	MS9154	Jennifer Chan, 8244
1	MS9154	Judy Lau, 8244
1	MS0899	Technical Library, 9536 (electronic copy)

